

# High- $T_c$ superconductivity above 130 K in cubic $MH_4$ compounds at ambient pressure

Xinxin Li,<sup>1,\*</sup> Weishuo Xu,<sup>1,\*</sup> Zengguang Zhou,<sup>1</sup> Jingming Shi,<sup>1</sup> Hanyu Liu,<sup>2</sup> Yue-Wen Fang,<sup>3,†</sup> Wenwen Cui,<sup>1,‡</sup> Yinwei Li,<sup>1,§</sup> and Miguel A. L. Marques,<sup>4,¶</sup>

<sup>1</sup>*Jiangsu Key Laboratory of Extreme Multi-Field Material Physics, School of Physics and Electronic Engineering, Jiangsu Normal University, Xuzhou 221116, China*

<sup>2</sup>*Key Laboratory of Material Simulation Methods and Software of Ministry of Education and State Key Laboratory of Superhard Materials, College of Physics, Jilin University, Changchun 130012, China*

<sup>3</sup>*Centro de Física de Materiales (CFM-MPC), CSIC-UPV/EHU, Manuel de Lardizabal Pasealekua 5, 20018 Donostia/San Sebastián, Spain*

<sup>4</sup>*Research Center Future Energy Materials and Systems of the University Alliance Ruhr and Interdisciplinary Centre for Advanced Materials Simulation, Ruhr University Bochum, Universitätsstraße 150, D-44801 Bochum, Germany*

(Dated: November 7, 2025)

Hydrides have long been considered promising candidates for achieving room-temperature superconductivity; however, the extremely high pressures typically required for high critical temperatures remain a major challenge in experiment. Here, we propose a class of high- $T_c$  ambient-pressure superconductors with  $MH_4$  stoichiometry. These hydrogen-based compounds adopt the *bcc*  $PtHg_4$  structure type, in which hydrogen atoms occupy the one-quarter body-diagonal sites of metal lattices, with the metal atoms acting as chemical templates for hydrogen assembly. Through comprehensive first-principles calculations, we identify three promising superconductors,  $PtH_4$ ,  $AuH_4$  and  $PdH_4$ , with superconducting critical temperatures of 84 K, 89 K, and 133 K, respectively, all surpassing the liquid-nitrogen temperature threshold of 77 K. The remarkable superconducting properties originate from strong electron-phonon coupling associated with hydrogen vibrations, which in turn arise from phonon softening in the mid-frequency range. Our results provide crucial insights into the design of high- $T_c$  superconductors suitable for future experiments and applications at ambient pressure.

## I. INTRODUCTION

The quest for high-temperature superconductors has been a central focus in condensed matter physics. Within the Bardeen-Cooper-Schrieffer (BCS) framework [1, 2], the superconducting critical temperature ( $T_c$ ) scales with the Debye frequency, which is typically high for light chemical elements. The metallic form of hydrogen, the lightest element, has been long proposed as a potential high- $T_c$  superconductor [3]. However, metallic hydrogen is notoriously difficult to realize in experiment, even under pressures approaching 500 GPa [4]. This challenge has redirected attention toward hydrogen-based compounds, where chemical precompression can significantly reduce the metallization pressure [5]. A landmark example is  $H_3S$ , which was predicted to exhibit a  $T_c$  of 203 K at 200 GPa [6, 7] and was subsequently confirmed experimentally as a high-temperature superconductor [8]. Recent advances in high-pressure synthesis have further expanded the family of hydride superconductors to include compounds such as  $LaH_{10}$  [9, 10],  $YH_6$  and  $YH_9$  [11, 12],  $CaH_6$  [13–15], as well as ternary hydrides including  $(La, Y)H_6$  [16],  $(La, Ce)H_9$  [17, 18],  $(La, Al)H_{10}$  [19]. In particular, a recent experimental study of  $LaSc_2H_{24}$  reported a  $T_c$  of 298 K at 260 GPa,

providing evidence of room-temperature superconductivity in reality.

Extreme pressures pose, however, significant experimental challenges, driving efforts to identify stable superconductors at lower or even ambient pressure. Representative examples include perovskites [20, 21], inverted perovskites [21], and perovskite-derived  $SM_2\text{-TM}\text{-}H_6$  [21–26], and other families with high-symmetry structures. In perovskite systems, compounds such as  $KInH_3$ ,  $SrAuH_3$ , and  $SrZnH_3$  have been predicted to exhibit high  $T_c$  values up to 132 K at ambient pressure [21, 27]. Du et al. predicted a series of high- $T_c$  superconductors below 10 GPa, with their best candidate having a maximum  $T_c$  of 170 K at 4 GPa, although these phases are thermodynamically metastable [28]. In spite of being a binary hydride, the cubic template  $M_4H$ , in which M is a metal element, also features a perovskite structure. Among such binary perovskite hydrides,  $Al_4H$  and  $Ag_4H$  have been predicted to show  $T_c$  of 54 and 63 K, respectively [21, 29, 30]. Compared to the aforementioned perovskites, the inverted perovskites tend to display moderate  $T_c$ . The machine-learning-aided searches have uncovered nearly 70 inverted perovskites with  $T_c$  ranging from 5 to 22 K [21, 31], while the current record is held by  $MgHCu_3$  which shows superconductivity at 42 K [32]. For the  $SM_2\text{-TM}\text{-}H_6$  family with vacancy-ordered perovskite structure [25], the critical temperature of superconducting  $Mg_2IrH_6$  is predicted to reach more than 77 K at ambient pressure [22, 24], and that of electron-doped  $Mg_2PtH_6$  can even surpass 100 K [22]. More recently, machine-learning assisted prediction has identified more high- $T_c$   $SM_2\text{-TM}\text{-}H_6$  hydrides at atmospheric

\* These authors contributed equally

† [yuewen.fang@ehu.eus](mailto:yuewen.fang@ehu.eus)

‡ [wenencui@jsnu.edu.cn](mailto:wenencui@jsnu.edu.cn)

§ [yinwei\\_li@jsnu.edu.cn](mailto:yinwei_li@jsnu.edu.cn)

¶ [miguel.marques@rub.de](mailto:miguel.marques@rub.de)

pressure such as  $\text{Li}_2\text{AuH}_6$  ( $T_c \sim 116$  K) and  $\text{Li}_2\text{AgH}_6$  ( $T_c \sim 108$  K) [23, 33]. Apart from these perovskite and peroskite-derived structures, the cubic  $\text{X}_4\text{H}_{15}$  systems offer another route to achieving ambient-pressure superconductivity, where hole doping can be strategically designed to both boost the  $T_c$  values up to 50 K and improve the thermodynamic stability [34].

Recently, the “chemical template concept” was proposed to successfully elucidate the mechanism of high- $T_c$  superconductivity in hydrides such as  $\text{CaH}_6$ ,  $\text{YH}_6$ ,  $\text{CeH}_9$ , and  $\text{LaH}_{10}$  [35]. In these systems, interstitial quasi-atoms (ISQs) exhibit an excellent structural match with the extended superhydrogen network embedded in the parent body- or face-centered cubic (*fcc*) metal lattice [35]. Building on this framework, some superconductors have been predicted recently. For example, incorporation of  $\text{H}_2$  units into *fcc*  $\text{NaK}$  framework led to the formation of  $\text{NaKH}_{12}$ , which displays a critical temperature of 246 K at 60 GPa [36]. In another case, hydrogen intercalation in the interstitial sites of sodium ion layers, combined with electronic matching to a honeycomb boron lattice, yielded a superconductor with a maximum  $T_c$  of 63 K at ambient pressure [37]. More recently, by integrating the “chemical template effect” with machine learning algorithms, Miao *et al.* identified 13 new structural prototypes and 31 thermodynamically stable metal superhydrides at pressures ranging from 100–300 GPa, among which 19 exhibiting  $T_c$  above 100 K [38]. These examples demonstrate that the chemical template concept provides a useful approach for designing new superconductors.

Within the framework of the chemical template concept, the high- $T_c$   $\text{CaH}_6$  and  $\text{YH}_6$  can be characterized as a combination of a *bcc* metal (e.g. Ca) with a hydrogen network where the hydrogen atoms occupy tetrahedral interstitial sites of the *bcc* lattice [35]. Such *bcc* metals are hereafter referred to as type I. In contrast, our analysis of the electron localization function (ELF) for a range of simple *bcc* metals reveals that, in some other cases such as Pt (denoted as type II), the interstitial electrons can occupy positions at around the one-quarter points along the body diagonals. The comparison of the ELF between the type-I and type-II metals are shown in Supplementary Fig. S1. Incorporation of hydrogen atoms into these one-quarter positions gives rise to a unexplored  $\text{PtHg}_4$ -type structure,  $\text{MH}_4$ .

In this study, guided by the concept of chemical template, high-throughput first-principles calculations have been used to predict a novel family of metal hydrides,  $\text{MH}_4$ , with a  $\text{PtHg}_4$ -type structure [39] where hydrogen atoms are bonded in the framework of *bcc* metals. In particular, we identify three ambient-pressure high- $T_c$  superconducting hydrides,  $\text{PtH}_4$ ,  $\text{AuH}_4$ , and  $\text{PdH}_4$ , with superconducting critical temperatures of 84 K, 89 K, and 133 K, respectively, all surpassing the boiling point of liquid nitrogen (77 K). In these  $\text{MH}_4$  superconductors, dynamical stability and enhanced superconductivity are closely related to the metallic lattice. These findings advance the search for high- $T_c$  superconductivity under am-

bient conditions and may open new avenues toward practical applications.

## II. COMPUTATIONAL DETAILS

Calculations were performed of the entire family of  $\text{PtHg}_4$ -type  $\text{MH}_4$  compounds, where M represents all the metal atoms in periodic table. Geometry relaxations, total energy calculations, and electronic properties were performed using the Vienna *Ab initio* Simulation Package (VASP) [41] using the projector augmented-wave (PAW) method. The exchange-correlation functional of density-functional theory was approximated by the generalized gradient approximation of Perdew, Burke, and Ernzerhof (PBE-GGA) [42]. The ion-electron interaction was described by PAW potentials with  $5d^96s^1$ ,  $4d^95s^1$ ,  $5d^{10}6s^1$  and  $1s^1$  electrons configurations as valence states for Pt, Pd, Au and H atoms, respectively. The cutoff energy for the expansion of the wave functions in the plane wave basis was set to 600 eV, with a grid of spacing  $2\pi \times 0.03 \text{ \AA}^{-1}$  for the electronic Brillouin zone integration [43]. In the high-throughput search, the dynamical stability was assessed by using the finite displacement and supercell method implemented in PHONOPY code [44]. *Ab initio* molecular dynamics simulations were performed in canonical (NVT) ensemble using a Nosé-Hoover thermostat [45] at 300 K. A time step of 1 fs and a total simulation time of 10 ps were used. The simulations employed a  $3 \times 3 \times 3$  supercell of the conventional unit cell containing 270 atoms.

To evaluate the superconducting properties, electron-phonon coupling (EPC) calculations were performed within Eliashberg theory for phonon-mediated superconductors under the Migdal approximation [46, 47]. Phonon spectra and EPC constants were obtained by density functional perturbation theory (DFPT) method using QUANTUM ESPRESSO [48–50]. PAW pseudopotentials from the PSlibrary [51] were used together with a kinetic energy cutoff of 90 Ry. The Brillouin zone was sampled using a  $24 \times 24 \times 24$   $k$ -point mesh and a  $6 \times 6 \times 6$   $q$ -point mesh for EPC calculations. A Gaussian smearing of 0.04 Ry was employed in evaluating EPC properties. The superconducting critical temperature was calculated by using Allen-Dynes equation [52] with a standard Coulomb pseudopotential  $\mu^* = 0.10$  [23, 53, 54]:

$$T_c = f_1 f_2 \frac{\omega_{\log}}{1.2} \exp \left[ \frac{-1.04(1 + \lambda)}{\lambda - \mu^*(1 + 0.62\lambda)} \right], \quad (1)$$

where  $\omega_{\log}$  is the logarithmic average frequency, and  $\lambda$  is the EPC parameter. The factors,  $f_1$  and  $f_2$  are strong-coupling correction and shape correction factors, respectively.

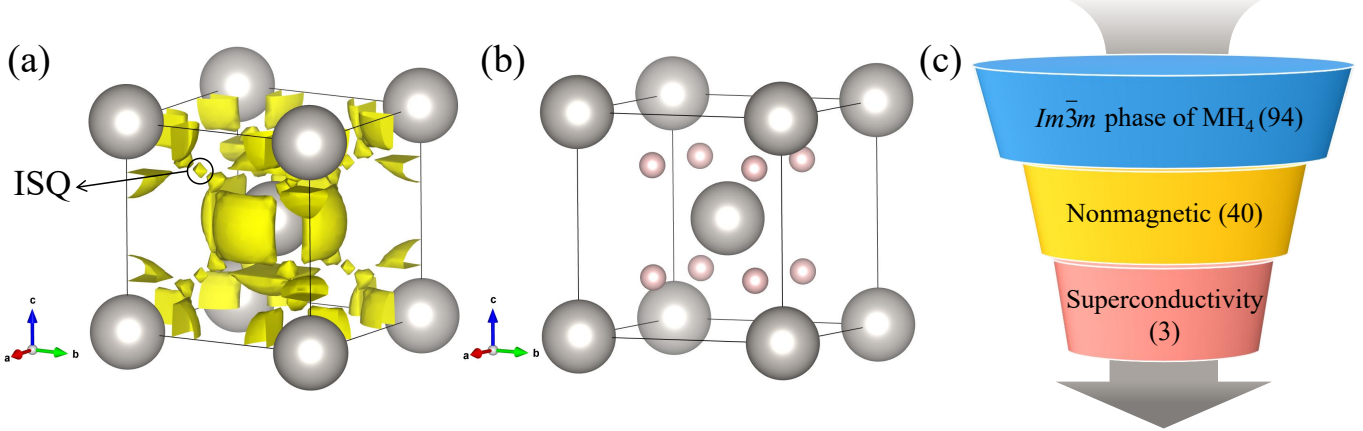


FIG. 1. (a) Three dimensional electron localization function of the *bcc* lattice formed by the M atoms (isosurface = 0.326). The circle highlights the interstitial quasi-atoms (ISQ). (b) The structure of MH<sub>4</sub> at ambient pressure. The M and H atoms are colored in gray and pink, respectively. (c) Schematic of our screening workflow. Panels (a) and (b) were produced with VESTA [40].

The isotropic Eliashberg equations take the form [55]:

$$[1 - Z(i\omega_n)]i\omega_n = -\frac{\pi}{\beta} \sum_{n'} \frac{Z(i\omega_{n'})i\omega_{n'}}{\Xi(i\omega_{n'})} \times \int \frac{2\omega a^2 F(\omega)}{(\omega_n - \omega_{n'})^2 + \omega^2} d\omega \quad (2)$$

$$\Phi(i\omega_n) = \frac{\pi}{\beta} \sum_{n'} \frac{\Phi(i\omega_{n'})}{\Xi(i\omega_{n'})} \times \left[ \int \frac{2\omega a^2 F(\omega)}{(\omega_n - \omega_{n'})^2 + \omega^2} d\omega - N_F \bar{V}_C \right] \quad (3)$$

$$\Phi(i\omega_n) = \Delta(i\omega_n)Z(i\omega_n) \quad (4)$$

$$\Xi(i\omega_n) = \sqrt{[Z(i\omega_n)\omega_n]^2 + [\Phi(i\omega_n)]^2} \quad (5)$$

where  $\Delta(i\omega_n)$  and  $Z(i\omega_n)$  represent superconducting gap and the renormalization function,  $N_F$  is the density of electronic states at the Fermi level, and  $\omega_n = (2n+1)\pi/\beta$  (with  $n$  integer) are the fermion Matsubara frequencies.

### III. RESULTS AND DISCUSSION

Unlike the valence electrons in type I metals (e.g., Ca, Y, and La), which tend to localize near the tetrahedral interstitial sites in the crystal lattice [35], the electrons in type II metals (e.g., Pt and Rh) exhibit pronounced delocalization around the one-quarter body-diagonal position of the *bcc* lattice,  $(\frac{1}{4}, \frac{1}{4}, \frac{1}{4})$ . This feature is clearly demonstrated by the ELF shown in Fig. 1(a) and Supplementary Figs. S1 and S2. In contrast to the hydrogen networks observed in superconducting hydrides such as CaH<sub>6</sub> and YH<sub>6</sub>, our calculations reveal that the intentional incorporation of hydrogen atoms into the electron-rich interstitial regions of these metals leads to the stabilization of a novel MH<sub>4</sub> structural framework. The re-

sulting MH<sub>4</sub> phases crystallize in the cubic structure with space group *Im* $\bar{3}m$ , adopting the PtHg<sub>4</sub>-type prototype. Structure-equivalent phases such as CrGa<sub>4</sub> and MnGa<sub>4</sub> have been experimentally synthesized and remain stable up to  $\sim$ 100 kbar [39]. In MH<sub>4</sub>, the M atoms occupy the Wyckoff 2a (0,0,0) positions corresponding to the corners and body center of the cubic cell, while the H atoms reside at the Wyckoff 8c ( $\frac{1}{4}, \frac{1}{4}, \frac{1}{4}$ ) sites. Each M atom is thus coordinated by eight equivalent H atoms in a *bcc*-like geometry, as illustrated in Fig. 1(b).

High-throughput first-principles screening was carried out for all MH<sub>4</sub> compounds with M spanning all the metal elements. The computational workflow of materials screening is schematically summarized in Fig. 1(c). This procedure identified three dynamically stable compounds: PdH<sub>4</sub>, PtH<sub>4</sub>, and AuH<sub>4</sub> (Fig. S3). In addition, these exhibit superconductivity with a  $T_c$  exceeding the boiling point of liquid nitrogen. To clarify the underlying superconducting mechanism, we first calculated their electronic band structures and densities of states (DOS), as shown in Figs. 2(a-c). Due to the chemical similarity of Pt and Pd, both compounds exhibit analogous electronic features. The *d* orbitals of the metal atoms dominate the DOS at the Fermi level ( $E_F$ ), contributing 0.18, 0.38 and 0.15 eV<sup>-1</sup> per primitive cell and accounting for 45%, 32% and 40% of the total DOS in PtH<sub>4</sub>, PdH<sub>4</sub> and AuH<sub>4</sub>, respectively. There is a significant overlap in partial DOS between metal and H atoms in the studied energy window from -4.5 to 4.5 eV, indicating that each pair of M–H is strongly hybridized.

As seen from the electron bands in Figs. 2(a,b) and the Fermi surfaces (FS) in Figs. 2(d,e), two bands, labeled #1 and #2, cross  $E_F$  in both PtH<sub>4</sub> and PdH<sub>4</sub>, forming two FS. Bands #1 and #2 are degenerate along the high-symmetry line from  $\Gamma$  to H in the first Brillouin zone. Band #1 exhibits a regular octahedral FS centered at the  $\Gamma$  point, whereas Band #2 consists of six inter-

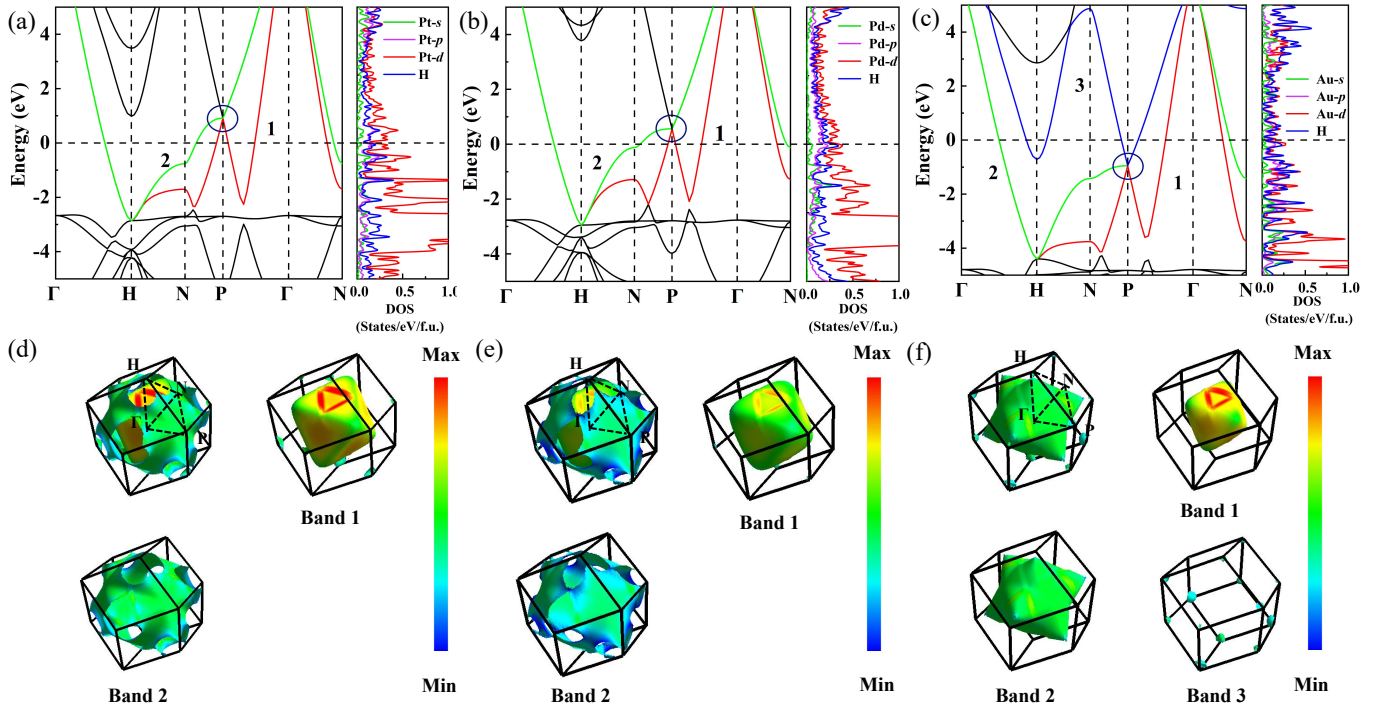


FIG. 2. Calculated band structures and projected density of states (PDOS) of (a-c) PtH<sub>4</sub>, PdH<sub>4</sub> and AuH<sub>4</sub> at 0 GPa. The circles highlight the triply degenerate (spinless) point where three energy bands meet together. (d-f) Fermi surfaces of PtH<sub>4</sub>, PdH<sub>4</sub> and AuH<sub>4</sub>, colored with respect to the Fermi velocity  $\langle v \rangle$  (10<sup>5</sup> m/s). The color bars use the same scale of  $\langle v \rangle$ .

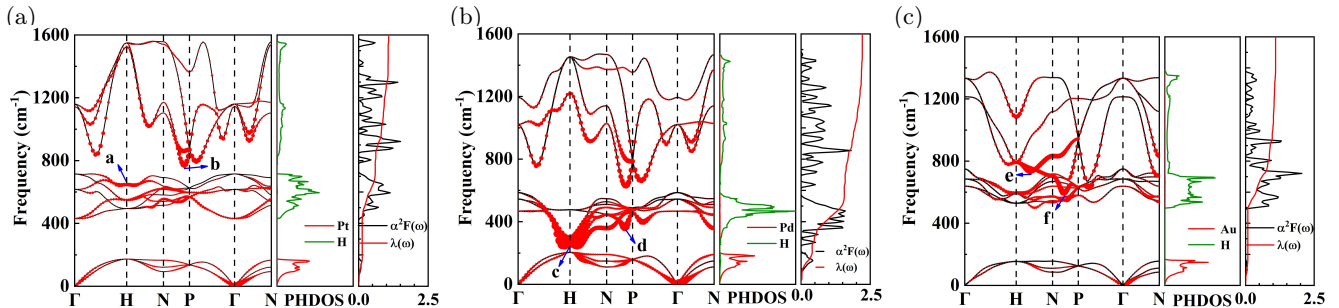


FIG. 3. Calculated phonon band structures, phonon density of states (PHDOS), electron-phonon coupling coefficient  $\lambda(\omega)$  and Elisberg spectral function  $\alpha^2 F(\omega)$  for (a) PtH<sub>4</sub>, (b) PdH<sub>4</sub>, and (c) AuH<sub>4</sub> at 0 GPa. The red solid circles show the phonon linewidth with a radius proportional to the EPC strength. The arrows denote the significant vibration modes in phonon dispersion curves.

connected, planar-quadrilateral-like Fermi sheets with a clover-shaped opening at the H point.

Since Au possesses one additional valence electron compared to Pt and Pd, Fig. 2(c) shows that the Fermi level in the band structure exhibits a distinct upward shift. Consequently, in the case of AuH<sub>4</sub>, three bands go across  $E_F$ , labeled as #1, #2, and #3, giving rise to the FS illustrated in Figs. 2(f). Band #1, similar to that in either PtH<sub>4</sub> or PdH<sub>4</sub>, forms a regular octahedral FS centered at the  $\Gamma$  point, whereas Band #2 generates a cuboidal FS with smoothly rounded faces and sharply protruding vertices. In contrast, Band #3 produces small Fermi pockets located at the H and P points of the Bril-

louin zone. Notably, the average Fermi velocity of PdH<sub>4</sub> is lower than those of both PtH<sub>4</sub> and AuH<sub>4</sub>, potentially suggesting stronger EPC and enhanced superconductivity [56].

To further study the lattice dynamics and electron-phonon coupling properties, we used the DFPT method to calculate the phonon dispersion curves, phonon density of states (PHDOS), and Eliashberg spectral function  $\alpha^2 F(\omega)$  for PtH<sub>4</sub>, PdH<sub>4</sub> and AuH<sub>4</sub>, as shown in Figs. 3(a-c), respectively. The values of the EPC constant ( $\lambda$ ), logarithmic average phonon frequency ( $\omega_{\log}$ ), and  $T_c$  are included in Table I. Using the Allen-Dynes equation with a Coulomb pseudopotential of 0.10, the

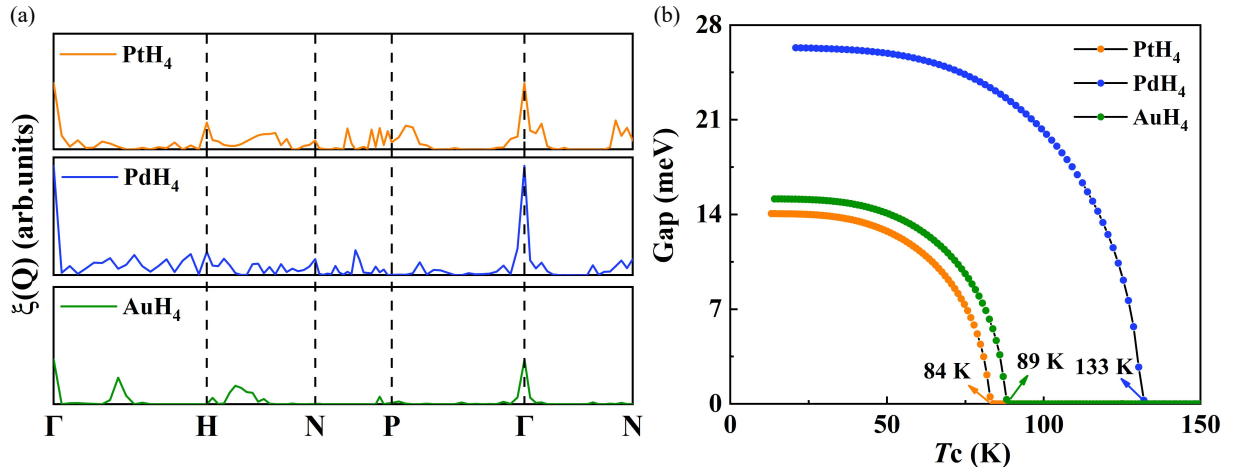


FIG. 4. (a) The calculated nesting function  $\xi(Q)$  of  $MH_4$  at 0 GPa along some particular  $q$  trajectories. (b) Isotropic superconducting gap of  $MH_4$  obtained by numerically solving the isotropic Migdal-Eliashberg equations.

TABLE I. The calculated EPC parameter ( $\lambda$ ), logarithmic average phonon frequency ( $\omega_{\log}$ ), and the estimated  $T_c$  for  $MH_4$  ( $M = Pd$ , Pt, and Au) at ambient pressures using the Allen-Dynes (AD) equations [52] or solving the Migdal-Eliashberg (ME) equations with  $\mu^* = 0.1$  [57].

Hydride	$\lambda$	$\omega_{\log}$ (K)	$T_c$ (K)	
			AD	ME
PtH <sub>4</sub>	1.08	892	75	84
PdH <sub>4</sub>	2.21	609	146	133
AuH <sub>4</sub>	1.14	873	79	89

ambient-pressure  $T_c$  for superconductivity are 75 K for  $PtH_4$ , 146 K for  $PdH_4$ , and 79 K for  $AuH_4$ . We also evaluated the values of  $T_c$  by solving self-consistently the isotropic Migdal-Eliashberg equations [57], which yields  $T_c$  values of 84 K, 133 K, and 89 K for  $PtH_4$ ,  $PdH_4$ , and  $AuH_4$ , respectively.

As seen in Fig. 3, the phonon dispersions of the three  $MH_4$  compounds can be roughly grouped into low-, medium-, and high-frequency regions based on the frequency distribution, where the low-lying phonons are dominated by metal atoms, and the latter two regions are exclusively from H atoms. In the cases of  $PtH_4$  and  $PdH_4$ , these three frequency regions are well separated. For  $PtH_4$ , the three vibrational regions contribute 12%, 44%, and 44% to the total electron-phonon coupling constant ( $\lambda = 1.08$ ). In contrast, for  $PdH_4$ , the gap between the low- and medium-frequency branches narrows significantly due to a prominent phonon softening at the H point. The softened modes at  $250 \sim 580 \text{ cm}^{-1}$  contributes 45% to the EPC strength, leading to a much larger  $\lambda$  value of 2.21.

Unlike the frequency distributions of  $PtH_4$  and  $PtH_4$ , the intermediate-frequency phonon modes touch the high-frequency modes in  $AuH_4$ . The intermediate-

frequency phonon modes ( $490 \sim 720 \text{ cm}^{-1}$ ) contribute 55% ( $\lambda = 0.63$ ) to the total  $\lambda$  1.14, and the high-frequency modes ( $720 \sim 1380 \text{ cm}^{-1}$ ) are responsible for 37% ( $\lambda = 0.42$ ) of the total  $\lambda$  1.14 in  $AuH_4$ .

The computational results reveal that the H vibrations dominate the Eliashberg spectral function  $\alpha^2 F(\omega)$ , providing the primary contribution to the total EPC strength. For the phonon modes showing significant phonon linewidths in Figs. 3(a-c), their detailed vibration patterns are shown in Fig. S5. All these vibration modes are dominated by the hydrogen atoms, indicating their crucial role in phonon softening and electron-phonon coupling.

Furthermore, the potential for Fermi surface nesting along the high-symmetry path was evaluated using the nesting function [58]:

$$\xi(\mathbf{Q}) = \frac{1}{N} \sum_{\mathbf{k}, i, j} \delta(\varepsilon_{\mathbf{k}, i} - \varepsilon_F) \delta(\varepsilon_{\mathbf{k} + \mathbf{Q}, j} - \varepsilon_F), \quad (6)$$

where  $\varepsilon_{\mathbf{k}, i}$  is the Kohn-Sham eigenvalue, and  $i, j$  are the indices of energy bands,  $N$  is the number of the  $k$  points, and  $\varepsilon_F$  is the Fermi Energy. As shown in the top panel of Fig. 4(a), the nesting function of  $PtH_4$  exhibits pronounced peaks along the H-N and H-P directions, corresponding to the phonon softening observed in Fig. 3(a). For  $PdH_4$ ,  $\xi(\mathbf{Q})$  exhibits several distinct peaks along the  $\Gamma$ -H and H-N paths [middle panel in Fig. 4(a)], which can be attributed to the Kohn anomalies near the H point [Fig. 3(b)]. These anomalies give rise to pronounced phonon softening [59]. In  $AuH_4$ , clear peaks are also present along the H-N direction. The large phonon linewidths near H-N further account for the strong peak observed along this path. These results of FS nesting, in combination with the analyses of phonon properties, are responsible for the strong EPC and high  $T_c$  in  $MH_4$ , in which the high  $T_c$  values are further confirmed by solving the isotropic Migdal-Eliashberg equations [Fig. 4(b)].

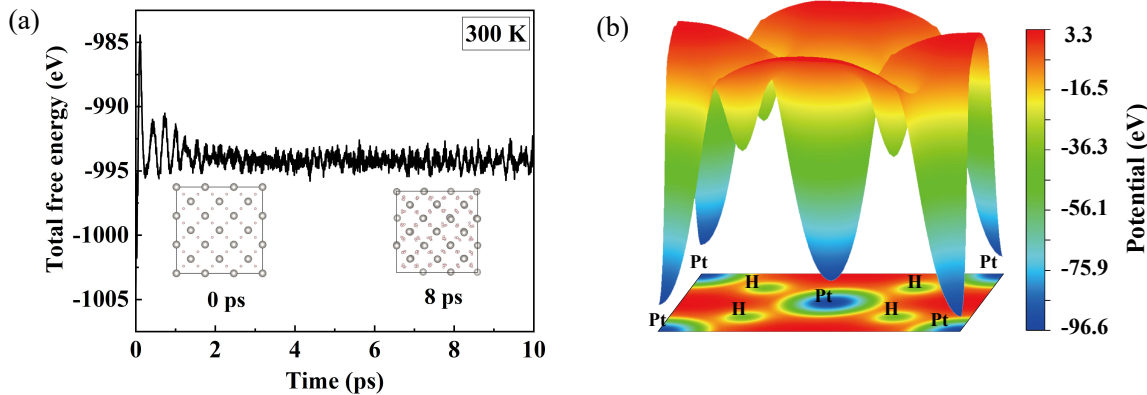


FIG. 5. (a) Ab initio molecular dynamics simulation of  $\text{PtH}_4$  at 0 GPa and 300 K. The inserts are snapshots of structures at 0 ps and 8 ps simulations, respectively. (b) Calculated electrostatic potential on the Pt–H plane.

Using  $\text{PtH}_4$  as an example, we further evaluate the kinetic stability of  $\text{MH}_4$  by performing the ab initio molecular dynamics simulations at 300 K. We find the supercell structure of  $\text{PtH}_4$  is well preserved without any structural collapse. As shown in Fig. 5(a), atomic displacements remain confined to small thermal fluctuations around equilibrium positions during a 10 ps trajectory, and the total Helmholtz free energy exhibits only minor variations after reaching the equilibrium state, confirming the absence of structural degradation. The electrostatic potential distribution on the (110) plane [Fig. 5(b)] further reveals that hydrogen atoms are strongly localized at the bottom of a deep potential well (-47 eV), suppressing proton diffusion and stabilizing the H sublattice [29, 32, 60].

Beyond  $\text{MH}_4$  ( $\text{M} = \text{Pt, Pd, and Au}$ ), where eight hydrogen atoms occupy the positions of ISQs of the M lattice, we systematically explored the introduction of  $\text{H}_n$  ( $n = 1\text{--}7$ ) at these sites (see Figs. S6–S8). However, among these configurations, only  $\text{PtH}_4$ ,  $\text{PdH}_4$  and  $\text{AuH}_4$  in the family of  $\text{MH}_4$  were found dynamically stable. Because Pt, Pd and Au all typically crystallize in the *fcc* structure (space group  $Fm\bar{3}m$ ) under ambient conditions, we also constructed hydrides based on the *fcc* lattice. Phonon calculations were performed for the resulting structures, and only the dynamically stable ones were evaluated for EPC properties. Whereas, none of them exhibited a high  $T_c$  (Figs. S9–S11). Of the hydrogenated *fcc* Pt structures (i.e.,  $\text{PtH}_n$  in which  $n$  runs from 1 to 8), only the  $Pn\bar{3}m$   $\text{Pt}_4\text{H}_2$  is dynamically stable and exhibits a small  $T_c$  of 0.16 K. The incorporation of hydrogen atoms into *fcc* Pd yields 10 dynamically stable structures. Among them,  $Fm\bar{3}m$   $\text{Pd}_4\text{H}_8$  has a  $T_c$  of 6.8 K, and the  $T_c$  values of the rest hydrides are all below 3 K. In contrast, no dynamically stable structures are found when H atoms are injected into the *fcc* lattice of Au. In addition, we find that substituting other transition metals except Pd/Pt/Au for M yielded no dynamically stable configurations.

In spite of the fact that the Pt, Pd and Au metals normally prefer crystallizing the closely packed *fcc* lat-

tice at ambient conditions, high temperature and pressure conditions have shown to make *bcc* lattice thermodynamically stable [61, 62]. Starting with a *bcc* structure could facilitate the synthesis of our proposed  $Im\bar{3}m$   $\text{MH}_4$ . Once the expected structures are formed, the high temperature and pressure can be gradually quenched to stabilize the superconducting  $\text{MH}_4$  at ambient pressure [23]. In addition, the employment of alloy may help release the requirements of hydride synthesis for pressures and temperatures. For example, a *bcc* TiFe-based hydride has been fabricated at only 5 GPa and 873 K through the hydrogenation of the TiFe alloy [63]. It is also noticed that the some nonequilibrium techniques such as electron-beam irradiation is able to drive the *fcc*-*bcc* transition in the Au thin films at ambient pressure [64]. This may also enable the possibility of synthesis of  $\text{MH}_4$  at ambient or near ambient pressure.

#### IV. CONCLUSIONS

In summary, we report a material family of high- $T_c$  hydrides,  $\text{MH}_4$ , stabilized at ambient pressure in the  $\text{PtHg}_4$ -type structure. Calculations of the electronic band structures, phonon spectra, and electron-phonon coupling predict  $T_c$  of 84 K, 133 K, and 89 K for  $\text{PtH}_4$ ,  $\text{PdH}_4$ , and  $\text{AuH}_4$ , respectively. The large EPC parameter  $\lambda_H$  and the pronounced phonon softening originate from hydrogen vibrations and strong Fermi surface nesting, which collectively enhance the superconductivity. These findings provide a viable pathway toward designing high- $T_c$  superconductors at ambient pressure, and suggest promising materials as touchstones for future experimental validation.

#### V. ACKNOWLEDGMENTS

The authors acknowledge funding from the NSFC under grants Nos. 12474012, 12574064, 12174160 and

12074154. W.C., and M.A.L.M. acknowledge the funding from the Sino-German Mobility Programme under Grant No. M-0362. Y.L. and J.S. acknowledge the funding from 333 High-level Talents Project of Jiangsu Province. W.C., Y.L., and H.L. acknowledge the funding from the Open Project of State Key Laboratory of High Pressure and Superhard Materials (Jilin University) (No. 202513). X.L. acknowledges the funding from Postgraduate Research & Practice Innovation Program of Jiangsu Province NO. 2025XKT0776. All the calculations were performed at the High Performance Computing Center of the School of Physics and Electronic Engineering of Jiangsu Normal University. Y.-W.F. acknowledges Extraordinary Grant of CSIC (Grant No. 2025ICT122) and the financial support received from the IKUR Strategy under the collaboration agreement between Ikerbasque Foundation and Centro de Física de Materiales (CFM-MPC) on behalf of the Department of Science, Universities and Innovation of the Basque Government (HPCAI21: AI-CrysPred). Y.-W.F. acknowledges enlightening discussions with his colleagues including D. Dančić and I. Errea. M.A.L.M. was supported by a grant from the Simons Foundation (SFI-MPS-NFS-00006741-12, P.T.) in the Simons Collaboration on New Frontiers

in Superconductivity and by the Kavli and the Klaus Tschira foundations as a part of the SuperC collaboration.

## VI. AUTHOR CONTRIBUTIONS

W.C., Y.L., Y.-W.F. and M.A.L.M. conceived the project. W.C., Y.L. and Y.-W.F. supervised the research. X.L., W.X., Y.-W.F., W.C. and M.A.L.M. performed the simulations and analyzed the data. X.L., W.X., Y.-W.F., Y.L., M.A.L.M. and W.C. co-wrote the manuscript; all authors discussed the results and commented on the manuscript.

## VII. DATA AVAILABILITY

The data supporting this study's findings are available within the article.

## VIII. DECLARATION OF INTERESTS

The authors declare no competing interests.

---

[1] J. Bardeen, L. N. Cooper, and J. R. Schrieffer, Theory of superconductivity, *Phys. Rev.* **108**, 1175 (1957).

[2] J. Bardeen, L. N. Cooper, and J. R. Schrieffer, Microscopic theory of superconductivity, *Phys. Rev.* **106**, 162 (1957).

[3] N. W. Ashcroft, Metallic hydrogen: A high-temperature superconductor?, *Phys. Rev. Lett.* **21**, 1748 (1968).

[4] M. I. Eremets, A. P. Drozdov, P. Kong, and H. Wang, Semimetallic molecular hydrogen at pressure above 350 gpa, *Nat. Phys.* **15**, 1246 (2019).

[5] N. Ashcroft, Hydrogen dominant metallic alloys: high temperature superconductors?, *Phys. Rev. Lett.* **92**, 187002 (2004).

[6] Y. Li, J. Hao, H. Liu, Y. Li, and Y. Ma, The metallization and superconductivity of dense hydrogen sulfide, *J. Chem. Phys.* **140** (2014).

[7] D. Duan, Y. Liu, F. Tian, D. Li, X. Huang, Z. Zhao, H. Yu, B. Liu, W. Tian, and T. Cui, Pressure-induced metallization of dense  $(\text{H}_2\text{S})_2\text{H}_2$  with high- $T_c$  superconductivity, *Sci. Rep.* **4**, 6968 (2014).

[8] A. Drozdov, M. Eremets, I. Troyan, V. Ksenofontov, and S. I. Shylin, Conventional superconductivity at 203 kelvin at high pressures in the sulfur hydride system, *Nature* **525**, 73 (2015).

[9] A. Drozdov, P. Kong, V. Minkov, S. Besedin, M. Kuzovnikov, S. Mozaffari, L. Balicas, F. F. Balakirev, D. Graf, V. Prakapenka, *et al.*, Superconductivity at 250 K in lanthanum hydride under high pressures, *Nature* **569**, 528 (2019).

[10] M. Somayazulu, M. Ahart, A. K. Mishra, Z. M. Geballe, M. Baldini, Y. Meng, V. V. Struzhkin, and R. J. Hemley, Evidence for superconductivity above 260 K in lanthanum superhydride at megabar pressures, *Phys. Rev. Lett.* **122**, 027001 (2019).

[11] H. Liu, I. I. Naumov, R. Hoffmann, N. Ashcroft, and R. J. Hemley, Potential high- $t_c$  superconducting lanthanum and yttrium hydrides at high pressure, *Proc. Natl. Acad. Sci. U. S. A.* **114**, 6990 (2017).

[12] F. Peng, Y. Sun, C. J. Pickard, R. J. Needs, Q. Wu, and Y. Ma, Hydrogen clathrate structures in rare earth hydrides at high pressures: possible route to room-temperature superconductivity, *Phys. Rev. Lett.* **119**, 107001 (2017).

[13] H. Wang, J. S. Tse, K. Tanaka, T. Iitaka, and Y. Ma, Superconductive sodalite-like clathrate calcium hydride at high pressures, *Proc. Natl. Acad. Sci. U. S. A.* **109**, 6463 (2012).

[14] L. Ma, K. Wang, Y. Xie, X. Yang, Y. Wang, M. Zhou, H. Liu, X. Yu, Y. Zhao, H. Wang, *et al.*, High-temperature superconducting phase in clathrate calcium hydride cah 6 up to 215 k at a pressure of 172 gpa, *Phys. Rev. Lett.* **128**, 167001 (2022).

[15] Z. Li, X. He, C. Zhang, X. Wang, S. Zhang, Y. Jia, S. Feng, K. Lu, J. Zhao, J. Zhang, *et al.*, Superconductivity above 200 k discovered in superhydrides of calcium, *Nat. Commun.* **13**, 2863 (2022).

[16] D. V. Semenok, I. A. Troyan, A. G. Ivanova, A. G. Kvashnin, I. A. Kruglov, M. Hanfland, A. V. Sadakov, O. A. Sobolevskiy, K. S. Pervakov, I. S. Lyubutin, *et al.*, Superconductivity at 253 K in lanthanum–yttrium ternary hydrides, *Mater. Today* **48**, 18 (2021).

[17] W. Chen, X. Huang, D. V. Semenok, S. Chen, D. Zhou, K. Zhang, A. R. Oganov, and T. Cui, Enhancement of superconducting properties in the La–Ce–H system at mod-

erate pressures, *Nat. Commun.* **14**, 2660 (2023).

[18] J. Bi, Y. Nakamoto, P. Zhang, K. Shimizu, B. Zou, H. Liu, M. Zhou, G. Liu, H. Wang, and Y. Ma, Giant enhancement of superconducting critical temperature in substitutional alloy (La, Ce)H<sub>9</sub>, *Nat. Commun.* **13**, 5952 (2022).

[19] S. Chen, Y. Qian, X. Huang, W. Chen, J. Guo, K. Zhang, J. Zhang, H. Yuan, and T. Cui, High-temperature superconductivity up to 223 K in the Al stabilized metastable hexagonal lanthanum superhydride, *Natl. Sci. Rev.* **11**, nwad107 (2024).

[20] Đorđe Dangić, Y.-W. Fang, T. F. Cerqueira, A. Sanna, T. Novoa, H. Gao, M. A. Marques, and I. Errea, **Ambient pressure high temperature superconductivity in RbPH<sub>3</sub> facilitated by ionic anharmonicity** (2025).

[21] T. F. Cerqueira, Y.-W. Fang, I. Errea, A. Sanna, and M. A. Marques, Searching materials space for hydride superconductors at ambient pressure, *Adv. Funct. Mater.* **34**, 2404043 (2024).

[22] A. Sanna, T. F. Cerqueira, Y.-W. Fang, I. Errea, A. Ludwig, and M. A. Marques, Prediction of ambient pressure conventional superconductivity above 80 K in hydride compounds, *npj Comput. Mater.* **10**, 44 (2024).

[23] K. Gao, T. F. Cerqueira, A. Sanna, Y.-W. Fang, Đ. Dangić, I. Errea, H.-C. Wang, S. Botti, and M. A. Marques, The maximum  $T_c$  of conventional superconductors at ambient pressure, *Nat. Commun.* **16**, 8253 (2025).

[24] K. Dolui, L. J. Conway, C. Heil, T. A. Strobel, R. P. Prasankumar, and C. J. Pickard, Feasible route to high-temperature ambient-pressure hydride superconductivity, *Phys. Rev. Lett.* **132**, 166001 (2024).

[25] A. Sanna, T. F. Cerqueira, E. D. Cubuk, I. Errea, and Y.-W. Fang, **Search for thermodynamically stable ambient-pressure superconducting hydrides in gnome database** (2025), [arXiv:2508.19781 \[cond-mat.supr-con\]](https://arxiv.org/abs/2508.19781).

[26] H. Xu, O. Schneble, R. Jaramillo, M. Polański, and J. Li, **Prediction of ambient-pressure high-temperature superconductivity in doped transition-metal hydrides** (2025), [arXiv:2507.19768 \[cond-mat.supr-con\]](https://arxiv.org/abs/2507.19768).

[27] B. Li, C. Zhu, J. Zhai, C. Yin, Y. Fan, J. Cheng, S. Liu, and Z. Shi, Theoretical prediction of high-temperature superconductivity in SrAuH<sub>3</sub> at ambient pressure, *Phys. Rev. B* **110**, 214504 (2024).

[28] M. Du, H. Huang, Z. Zhang, M. Wang, H. Song, D. Duan, and T. Cui, High-temperature superconductivity in perovskite hydride below 10 gpa, *Adv. Sci.* **11**, 2408370 (2024).

[29] Y. He, J. Lu, X. Wang, and J.-j. Shi, Phonon-mediated superconductivity in the metal-bonded perovskite Al<sub>4</sub>H up to 54 K under ambient pressure, *Phys. Rev. B* **108**, 054515 (2023).

[30] C. Tian, J.-j. Shi, P. Wang, J. Du, J. Lu, X. Wang, Y.-h. Zhu, and H.-x. Zhong, Ambient-pressure topological superconductivity in Ag<sub>4</sub>H up to 63 K by metallization of hydrogen, *Phys. Rev. B* **111**, 094521 (2025).

[31] N. Hoffmann, T. F. Cerqueira, J. Schmidt, and M. A. Marques, Superconductivity in antiperovskites, *npj Comput. Mater.* **8**, 150 (2022).

[32] C. Tian, Y. He, Y.-h. Zhu, J. Du, S.-m. Liu, W.-h. Guo, H.-x. Zhong, J. Lu, X. Wang, and J.-j. Shi, Few-hydrogen metal-bonded perovskite superconductor MgHCu<sub>3</sub> with a critical temperature of 42 k under atmospheric pressure, *Adv. Funct. Mater.* **34**, 2304919 (2024).

[33] Z. Ouyang, B.-W. Yao, X.-Q. Han, P.-J. Guo, Z.-F. Gao, and Z.-Y. Lu, High-temperature superconductivity in Li<sub>2</sub>AuH<sub>6</sub> mediated by strong electron-phonon coupling under ambient pressure, *Phys. Rev. B* **111**, L140501 (2025).

[34] K. Gao, W. Cui, T. F. Cerqueira, H.-C. Wang, S. Botti, and M. A. Marques, Enhanced superconductivity in X<sub>4</sub>H<sub>15</sub> compounds via hole-doping at ambient pressure, *Adv. Sci.* , e08419 (2025).

[35] Y. Sun and M. Miao, Chemical templates that assemble the metal superhydrides, *Chem* **9**, 443 (2023).

[36] W. Zhao, A. Ellis, D. Duan, H. Wang, Q. Jiang, M. Du, T. Cui, and M. Miao, Unlocking the origin of high-temperature superconductivity in molecular hydrides at moderate pressures, *Adv. Funct. Mater.* **35**, 2415910 (2025).

[37] W. Zhao, D. Duan, Z. Liu, Z. Huo, S. Guo, D. An, M. Miao, and T. Cui, High temperature superconductor na2b2h stabilized by hydrogen intercalation under ambient pressure, *Sci. China:Phys., Mech. Astron.* **67**, 118211 (2024).

[38] Y. Sun, A. Ellis, X. Chen, and M. Miao, Batch discovery of complex metal superhydrides via an effective machine learning method structured by chemical template concept, *J. Am. Chem. Soc.* (2025).

[39] U. Häussermann, P. Viklund, M. Boström, R. Norrestam, and S. Simak, Bonding and physical properties of humerothery compounds with the PtHg<sub>4</sub> structure, *Phys. Rev. B* **63**, 125118 (2001).

[40] K. Momma and F. Izumi, **VESTA: a three-dimensional visualization system for electronic and structural analysis**, *Journal of Applied Crystallography* **41**, 653 (2008).

[41] G. Kresse and J. Furthmüller, Efficient iterative schemes for ab initio total-energy calculations using a plane-wave basis set, *Phys. Rev. B* **54**, 11169 (1996).

[42] J. P. Perdew, Generalized gradient approximation made simple, *Phys. Rev. Lett.* **77**, 3868 (1997).

[43] W. Tang, E. Sanville, and G. Henkelman, A grid-based bader analysis algorithm without lattice bias, *J. Phys.:Condens. Matter* **21**, 084204 (2009).

[44] A. Togo and I. Tanaka, First principles phonon calculations in materials science, *Scr. Mater.* **108**, 1 (2015).

[45] D. J. Evans and B. L. Holian, The nose-hoover thermostat, *J. Chem. Phys.* **83**, 4069 (1985).

[46] Q. Li, S. Han, X. Zhang, S. Ding, A. Bergara, and G. Yang, Extended hydrogen frameworks in nonmetallic superhydrides enabling 190 K superconductivity, *Superconductivity* , 100196 (2025).

[47] S. Han, A. Bergara, X. Zhang, S. Ding, F. Li, and G. Yang, Pressure-driven charge transfer and tunable superconductivity in intermetallic Li-Mg electrides, *Superconductivity* , 100187 (2025).

[48] P. Giannozzi, S. Baroni, N. Bonini, M. Calandra, R. Car, C. Cavazzoni, D. Ceresoli, G. L. Chiarotti, M. Cococcioni, I. Dabo, *et al.*, Quantum espresso: a modular and open-source software project for quantum simulations of materials, *J. Phys.:Condens. Matter* **21**, 395502 (2009).

[49] P. Giannozzi, O. Andreussi, T. Brumme, O. Bunau, M. B. Nardelli, M. Calandra, R. Car, C. Cavazzoni, D. Ceresoli, M. Cococcioni, *et al.*, Advanced capabilities for materials modelling with quantum espresso, *J. Phys.:Condens. Matter* **29**, 465901 (2017).

[50] P. Giannozzi, O. Baseggio, P. Bonfà, D. Brunato, R. Car, I. Carnimeo, C. Cavazzoni, S. De Gironcoli, P. Delugas,

F. Ferrari Ruffino, *et al.*, Quantum espresso toward the exascale, *J. Chem. Phys.* **152** (2020).

[51] A. Dal Corso, Pseudopotentials periodic table: From H to Pu, *Comput. Mater. Sci.* **95**, 337 (2014).

[52] P. B. Allen and R. Dynes, Transition temperature of strong-coupled superconductors reanalyzed, *Phys. Rev. B* **12**, 905 (1975).

[53] K. Gao, W. Cui, J. Shi, A. P. Durajski, J. Hao, S. Botti, M. A. L. Marques, and Y. Li, Prediction of high- $T_c$  superconductivity in ternary actinium beryllium hydrides at low pressure, *Phys. Rev. B* **109**, 014501 (2024).

[54] Y.-W. Fang and I. Errea, Superconductivity in barium hydrides via incorporation of light elements, *Phys. Rev. B* **112**, 125204 (2025).

[55] P. B. Allen and B. Mitrović, Theory of superconducting  $T_c$ , *Solid State Phys.* **37**, 1 (1983).

[56] T. Kiss, T. Yokoya, A. Chainani, S. Shin, T. Hanaguri, M. Nohara, and H. Takagi, Charge-order-maximized momentum-dependent superconductivity, *Nat. Phys.* **3**, 720 (2007).

[57] G. Eliashberg, Interactions between electrons and lattice vibrations in a superconductor, *Sov. Phys. JETP* **11**, 696 (1960).

[58] J. Tse, Y. Yao, and K. Tanaka, Novel superconductivity in metallic snh 4 under high pressure, *Phys. Rev. Lett.* **98**, 117004 (2007).

[59] D. Kasinathan, J. Kuneš, A. Lazicki, H. Rosner, C.-S. Yoo, R. Scalettar, and W. Pickett, Superconductivity and lattice instability in compressed lithium from fermi surface hot spots, *Phys. Rev. Lett.* **96**, 047004 (2006).

[60] Y. He, J. Du, S.-m. Liu, C. Tian, M. Zhang, Y.-h. Zhu, H.-x. Zhong, X. Wang, and J.-j. Shi, Metal-bonded perovskite lead hydride with phonon-mediated superconductivity exceeding 46 K under ambient pressure, *J. Phys.:Condens. Matter* **36**, 205502 (2024).

[61] N. A. Smirnov, Relative stability of cu, ag, and pt at high pressures and temperatures from ab initio calculations, *Phys. Rev. B* **103**, 064107 (2021).

[62] S. R. Baty, L. Burakovskiy, D. J. Luscher, S. Anzellini, and D. Errandonea, Palladium at high pressure and high temperature: A combined experimental and theoretical study, *Journal of Applied Physics* **135**, 075103 (2024).

[63] N. Endo, H. Saitoh, A. Machida, and Y. Katayama, Formation of bcc tife hydride under high hydrogen pressure, *International Journal of Hydrogen Energy* **38**, 6726 (2013).

[64] S. B. Lee, J. Jung, and H. N. Han, Transition to body-centered cubic structure in au thin films under electron-beam irradiation, *Acta Materialia* **247**, 118759 (2023).